PRAMANA — journal of physics

Vol. 79, No. 1
July 2012
pp. 151–163

AlGaN/GaN-based HEMT on SiC substrate for microwave characteristics using different passivation layers

T R LENKA* and A K PANDA
National Institute of Science and Technology (NIST), Palur Hills, Berhampur 761 008, India
*Corresponding author. E-mail: trlenka@gmail.com

MS received 10 August 2010; revised 23 January 2012; accepted 8 February 2012

Abstract. In this paper, a new gate-recessed AlGaN/GaN-based high electron mobility transistor (HEMT) on SiC substrate is proposed and its DC as well as microwave characteristics are discussed for Si_3N_4 and SiO_2 passivation layers using technology computer aided design (TCAD). The two-dimensional electron gas (2DEG) transport properties are discussed by solving Schrödinger and Poisson equations self-consistently resulting in various subbands having electron eigenvalues. From DC characteristics, the saturation drain currents are measured to be 600 mA/mm and 550 mA/mm for Si_3N_4 and SiO_2 passivation layers respectively. Apart from DC, small-signal AC analysis has been done using two-port network for various microwave parameters. The extrinsic transconductance parameters are measured to be 131.7 mS/mm at a gate voltage of $V_{gs} = -0.35$ V and 114.6 mS/mm at a gate voltage of $V_{gs} = -0.4$ V for Si_3N_4 and SiO_2 passivation layers respectively. The current gain cut-off frequencies (f_t) are measured to be 27.1 GHz and 23.97 GHz in unit-gain-point method at a gate voltage of -0.4 V for Si_3N_4 and SiO_2 passivation layers respectively. Similarly, the power gain cut-off frequencies (f_{max}) are measured to be 41 GHz and 38.5 GHz in unit-gain-point method at a gate voltage of -0.1 V for Si_3N_4 and SiO_2 passivation layers respectively. Furthermore, the maximum frequency of oscillation or unit power gain (MUG = 1) cut-off frequencies for Si_3N_4 and SiO_2 passivation layers are measured to be 32 GHz and 28 GHz respectively from MUG curves and the unit current gain, $|h_{21}| = 1$ cut-off frequencies are measured to be 140 GHz and 75 GHz for Si_3N_4 and SiO_2 passivation layers respectively from the *abs* $|h_{21}|$ curves. HEMT with Si_3N_4 passivation layer gives better results than HEMT with SiO_2 passivation layer.

Keywords. Two-dimensional electron gas; high electron mobility transistor; heterojunction; microwave; nitride; passivation.

PACS Nos 81.05.Ea; 73.40.Kp; 79.60.Jv; 74.78.Fk

1. Introduction

The AlGaN/GaN-based high electron mobility transistors (HEMTs) are attracting much research interest worldwide because of their high density of states (DOS), high electron saturation drift velocity, large band gap, high breakdown voltage, high electric field

strength and good thermal stability [1–8]. Apart from this, AlGaN/GaN heterojunction has large conduction band discontinuity and strong inherent spontaneous and piezoelectric polarization effects resulting in a high concentration of two-dimensional electron gas (2DEG) or quantum well (QW) at the heterointerface [3,4]. Consequently, with the excellent epitaxial material properties and improved process techniques, GaN-based devices can demonstrate power density 5–10 times larger than that of the GaAs-based devices [4,5]. The AlGaN/GaN high electron mobility transistors (HEMT) display large potential in high-frequency, high-temperature and large-power fields [6,7]. Furthermore, SiC as a substrate provides an excellent thermal conductivity of 120 W/m-K [8,9]. This is beneficial for effective heat removal in high power applications. The power performance of AlGaN/GaN HEMT grown on SiC substrates is 9.1 W/mm at 8.2 GHz with the total power extracted from a single device of 9.8 W at this frequency [10]. A power added efficiency of 77% (1.7 W/mm) at 4 GHz was reported for a 0.5 mm periphery HEMT grown on a sapphire substrate [10].

The current collapse in AlGaN/GaN HEMTs is due to the presence of slow-acting trapping states between the gate and the drain of the device. These trapping states are assumed to be associated with surface states created by dangling bonds, threading dislocations accessible at the surface and ions absorbed from the ambient environment [10,11]. These states trap electrons injected by the gate and create a layer of charge at or near the surface that depletes the channel in the high field region between the gate and the drain. Due to the small time constant of the trapping states, it is not possible for the electrons to modulate the channel charge during large signal RF operation, which results in reduced RF current swing and output power.

However, this degradation can be reduced significantly, if the HEMT surface is passivated with suitable dielectric materials. Surface passivation of undoped AlGaN/GaN HEMTs eliminates the surface effects which are responsible for limiting both the RF current and breakdown voltages of the devices [11]. In this work, we have considered Si_3N_4 and SiO_2 dielectrics as passivation layers. The thermal conductivity of Si_3N_4 (0.37 W/cm K) is approximately the same as that of sapphire (0.42 W/cm K) and it does not change the thermal resistance of the device whereas the thermal conductivity of SiO_2

Table 1. Properties of silicon dioxide (SiO_2) and silicon nitride (Si_3N_4) at 300 K.

Properties	SiO_2	Si_3N_4
Structure	Amorphous	Amorphous
Melting point (°C)	$\sim$ 1600	1900
Density (g/cm^3)	2.2	3.1
Refractive index	1.46	2.05
Dielectric constant	3.9	7.5
Dielectric strength (V/cm)	10^7	10^7
Infrared absorption band (μm)	9.3	11.5–12.0
Energy gap at 300 K (eV)	9	$\sim$ 5.0
Thermal conductivity (W/cm K)	0.014	0.37
DC resistivity at 25°C (Ω-cm)	10^{14}–10^{16}	$\sim 10^{14}$
DC resistivity at 500°C (Ω-cm)	–	2×10^{13}
Etch rate in buffered HF (Å/min)	1000	5–10

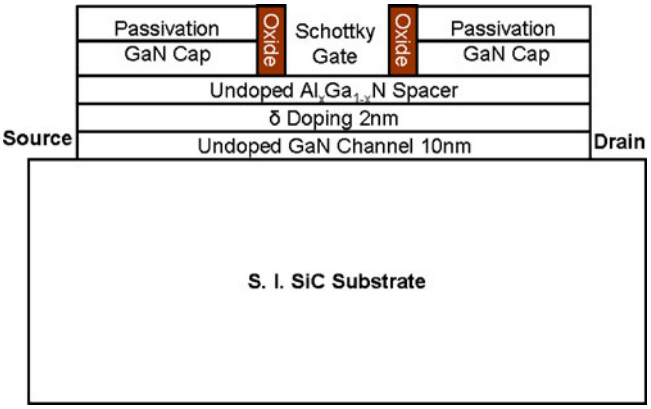

Figure 1. Simplified structure of the proposed AlGaN/GaN-based HEMT on SiC substrate.

is 0.01 W/cm K [12]. From the material properties presented in table 1, it seems that Si_3N_4 can act as a better passivation layer. However, a detailed study is necessary for the evaluation of its performance.

Further, RF power recovery after passivation using Si_3N_4 shows an average increase of the maximum power by a factor of 3 [12,13]. According to the trap theory, this improvement is mainly due to the reduction of electrically active surface traps. However, due to the spontaneous polarization on the 2DEG carrier concentration, the mechanical strain of the passivation layer might influence device performance [13]. This type of preliminary study is seen in [1–13]. Keeping all these in mind, the authors characterize the AlGaN/GaN-based HEMT on SiC semi-insulating substrate by deploying two different passivation layers such as Si_3N_4 and SiO_2 over the stacked layers of the device for its performance evaluation. The schematic diagram of this proposed device structure is shown in figure 1.

The design of the proposed gate-recessed HEMT structure, its physics and the simulation model are discussed in §2. The 2DEG transport properties which include the subband calculation by self-consistent solution of Poisson and Schrödinger equations by effective mass approximation (EMA) and 2DEG density of the proposed heterostructure are discussed in §3. The results and discussion include DC and microwave characteristics such as transconductance (g_m), cut-off frequency (f_t), maximum frequency of oscillation (f_{max}), maximum available/stable gain (MAG/MSG), Rollett stability factor (K) and Masons unilateral gain (MUG) in §4. Conclusion is drawn in §5.

2. HEMT structure and its simulation model

The proposed gate-recessed AlGaN/GaN HEMT, which consists of several stacked layers, is generally grown by molecular beam epitaxy (MBE) or metal-organic chemical vapour deposition (MOCVD) technique [8–13] as shown in figure 1. The proposed structure consists of a SiC semi-insulating substrate of 0.8 μm thickness. An undoped GaN channel layer of 10 nm thickness is grown over the SiC substrate followed by delta doping

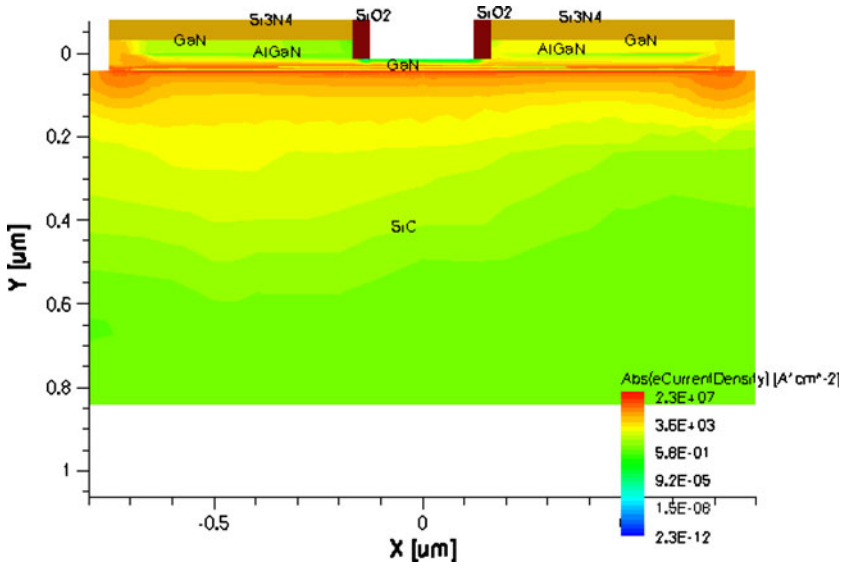

Figure 2. Simulated structure of the proposed AlGaN/GaN-based HEMT on SiC substrate.

and growth of undoped $Al_{0.3}Ga_{0.7}N$ spacer layer of 0.0345 μm thickness. Further delta doping is done by introducing a sheet charge of 5.4×10^{12} cm^{-2} at a depth of 0.031 μm of the $Al_{0.3}Ga_{0.7}N$ layer. Moreover, doped GaN layer of 0.03 μm thickness is deployed for the cap layer of the device [7,14]. To reduce the RF-power level degradation, insulated

Table 2. The structural parameters of the proposed $Al_xGa_{1-x}N$/GaN-based HEMT on SiC substrate.

Parameter	Value
Height of SiC substrate	0.8 μm
Height of GaN channel	10 nm
Height of $Al_xGa_{1-x}N$ spacer	0.0345 μm
Delta doping thickness	2 nm
Height of GaN cap layer	0.03 μm
Gate length (L_g)	0.25 μm
Contact length (L_c)	0.05 μm
Gate recess	0.015 μm
Width of the oxide spacer	0.04 μm
Width of the trap	0.03 μm
Height of the top passivation	0.05 μm
Sheet charge density	5.4×10^{12} cm^{-2}
x mole fraction ($Al_xGa_{1-x}N$)	0.3

Si_3N_4 and SiO_2 passivation layers of 0.05 μm thickness are deployed. The deposition of the passivation layer is generally done before the Schottky gate contact [14] and the simulated structure of the proposed gate-recessed HEMT is shown in figure 2. The structural parameters of the device are mentioned in table 2.

Better coverage of the passivation layer gives less dispersion, high gain and high breakdown voltage in submicron devices and improves its performance [15]. We have considered the gate length (L_g) of the device as 0.25 μm. The source and drain contact lengths are 0.05 μm each [14,15]. In this model, the gate is recessed to a depth of 0.015 μm and the barrier height of the Schottky-gate is 0.9 eV. The oxide spacer of 0.04 μm thickness is used as stress reliever which acts as sidewalls of the Schottky-gate contact. Further hydrodynamic transport model is considered for the simulation by incorporating various mobility models such as doping dependence and carrier temperature-driven high field saturation model. Various recombination models such as Auger, Shockley–Read–Hall (SRH) and radiative recombination process are considered in the simulation model [14–17].

3. 2DEG Transport properties

$Al_{0.3}Ga_{0.7}N$ is a wide band-gap semiconductor of energy gap, $E_g = 4.24$ eV and GaN has a comparatively lesser band gap than AlGaN having energy gap, $E_g = 3.4$ eV. The growth of a wide band-gap material over a narrow band-gap material creates a two-dimensional electron gas (2DEG) at the heterointerface, so that confinement of electrons in the quantum well is possible, which leads to higher electron mobility resulting in a high speed device [4–7]. Better modulation of the 2DEG density results in high current gain cut-off frequency (f_t). Here effective mass approximation is used to calculate the subband structure in the 2DEG, formed at the $Al_{0.3}Ga_{0.7}N$/GaN heterointerface [7,14]. In this heterostructure, Schrödinger wave equation and Poisson equation are self-consistently solved incorporating both heavy holes and light holes in the simulation model which results in various subbands having electron eigenenergy E_i and eigenvalues λ. The flow diagram of solving Poisson and Schrödinger equations self-consistently is shown in figure 3. The solution indicates that $\psi_i(x)$ might have infinite dependent solutions. However, we have considered nine subbands and the corresponding electron eigenvalues are given in table 3. The one-dimensional electron concentration $n(x)$ is related by the wave function and number of electrons per unit area for each energy state and is given by [16,17]:

$$n(x) = \sum_i N_i \, |\psi_i(x)|^2, \tag{1}$$

where N_i is the number of electrons per unit area for each energy state E_i and wave function ψ_i of the ith state and the presentation of energy states are shown in figure 4. However, the 2DEG density, n_s, of the AlGaN/GaN HEMT is derived as [17]

$$n_s = \frac{\sigma_{\mathrm{AlGaN}} \cdot t_{\mathrm{AlGaN}} - (\varepsilon\varepsilon_0/q)\phi_{\mathrm{B}} + (\varepsilon\varepsilon_0/q^2)(\Delta E_{c,\mathrm{AlGaN}})}{t_{\mathrm{AlGaN}} + d_0}, \tag{2}$$

where σ_{AlGaN} is the polarization charge density, t_{AlGaN} is the thickness of the AlGaN layer, $\Delta E_{c,\,\mathrm{AlGaN}}$ is the conduction band discontinuity, d_0 is the thickness of the spacer layer and

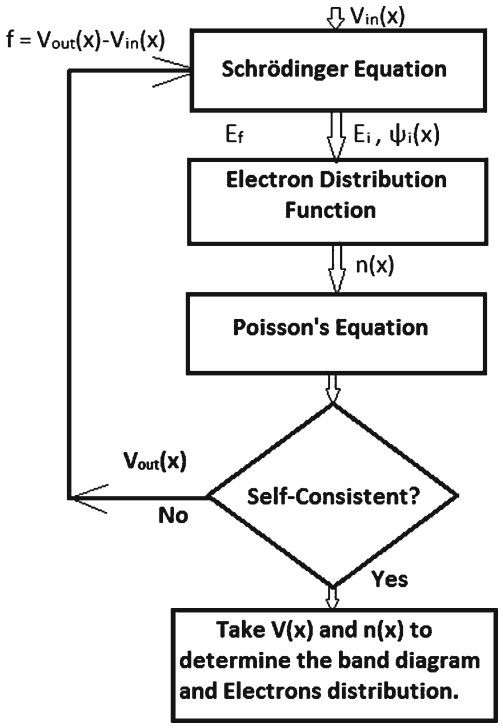

Figure 3. Flow chart showing the self-consistent solution of Poisson and Schrödinger equations in the $Al_{0.3}Ga_{0.7}N/GaN$ HEMT structure.

all other terms have the usual meaning. The electron concentration in terms of subbands in the 2DEG is shown in figure 4 and it is realized that the 2DEG is formed at a distance of 450 Å from the surface of the heterostructure.

Table 3. Eigenvalues of various subbands.

Eigenvalues	Energy (eV)
Electron eigenvalue 1	−1.719900e−01
Electron eigenvalue 2	−1.214861e−02
Electron eigenvalue 3	4.209814e−02
Electron eigenvalue 4	6.876351e−02
Electron eigenvalue 5	8.545898e−02
Electron eigenvalue 6	9.743659e−02
Electron eigenvalue 6	1.069035e−01
Electron eigenvalue 8	1.148511e−01
Electron eigenvalue 9	1.213420e−01

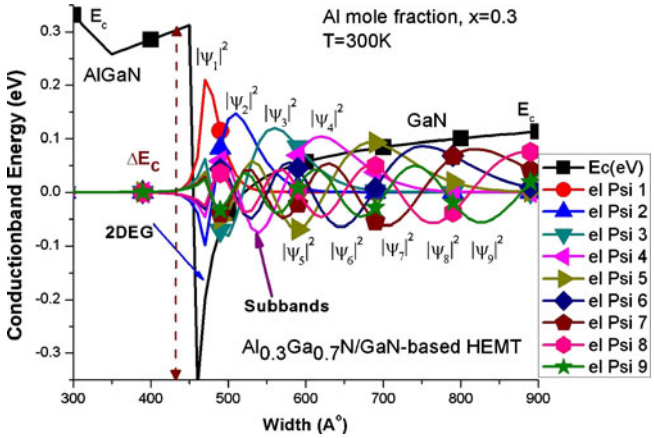

Figure 4. Formation of 2DEG with subbands for different electron eigenvalues.

4. Results and discussion

4.1 *DC Characteristics*

Different insulating passivation layers such as Si_3N_4 and SiO_2 of 0.05 μm thickness have been deployed for the performance evaluation of the proposed heterostructure device. The DC characteristics of the device is measured from TCAD and the conditions of the I–V characteristics measurement are $-5\ \text{V} < V_{\text{gs}} < 0.8\ \text{V}$ and $0\ \text{V} < V_{\text{ds}} < 1\ \text{V}$, where V_{gs} is the gate voltage and V_{ds} is the source–drain voltage. It is seen in figure 5, that the maximum drain current of the proposed HEMT is measured to be 290.2 mA/mm

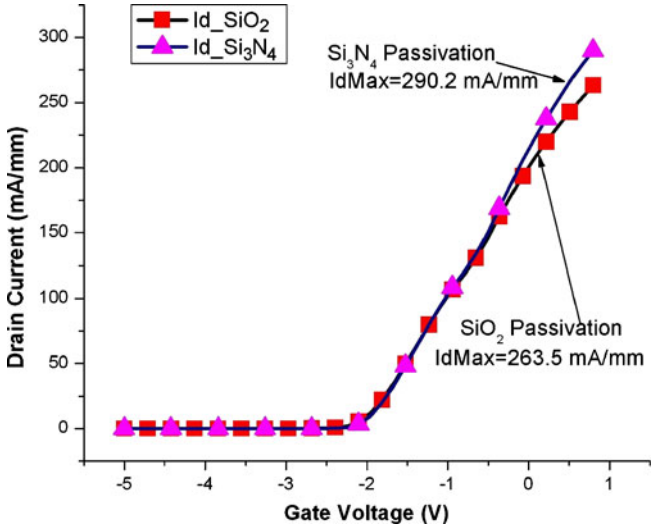

Figure 5. Gate characteristics for Si_3N_4 and SiO_2 passivation layers.

and 263.5 mA/mm for Si_3N_4 passivation and SiO_2 passivation layer respectively. The pinch-off voltage of the device is almost −2 V as shown in the gate characteristics.

Moreover, it can be seen from the drain characteristics (shown in figure 6), that the drain current of the SiC-based GaN HEMT device does not decrease as the drain–source voltage increases. The device is simulated by varying the drain voltage from 0 V to 5 V for gate voltages from −0.8 V to 0.8 V. The maximum saturation drain current of the HEMT device are measured to be 600 mA/mm and 550 mA/mm for Si_3N_4 passivation layer and SiO_2 passivation layer respectively. This improvement in drain current is due to the fact that the SiC substrate exhibits better thermal conduction performance when Si_3N_4 passivation layer is used, which leads to small thermal resistance and improved overall performance of the device. Furthermore, the rise in current is due to an increase in positive charge at the Si_3N_4/GaN interface, resulting in a higher sheet carrier concentration in the channel [10].

4.2 *Microwave characteristics*

The microwave characteristics are discussed with the help of two-port network analysis [17,18]. Using the same biasing and sweeping scheme as that of DC, the small-signal characteristics are analysed for various frequencies. A mixed-mode environment is created for the AC simulation instead of simulating an isolated HEMT. That is, HEMT is embedded into an external circuit forming a two-port network, as shown in figure 7. Here the voltage sources are attached to the gate (port 1) and drain (port 2) terminals. All other terminals are grounded. The small-signal output file contains the admittance (A) and capacitance (C) matrices [17], which are equivalent to the Y-matrix as $Y = A + j\omega C$. The rows and columns of the matrices are given by the nodes in the small-signal analysis. Y-matrix obtained now can be converted to any other matrix such as S, Z or h-matrix as per suitability and the microwave parameters such as transconductance (g_m), cut-off frequency (f_t), maximum frequency of oscillation (f_{max}), maximum available/stable gain

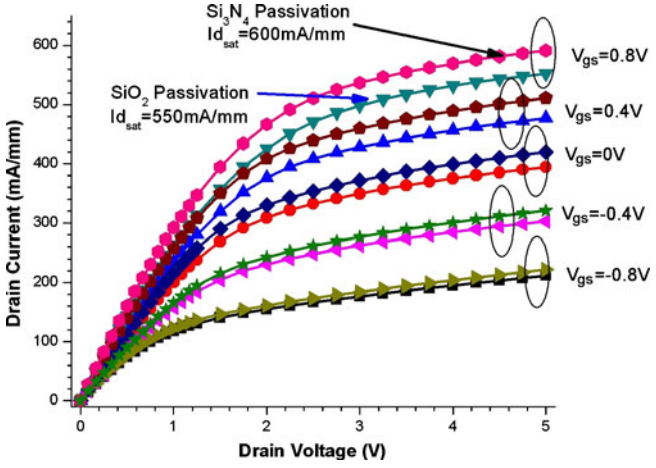

Figure 6. Drain characteristics for Si_3N_4 and SiO_2 passivation layers.

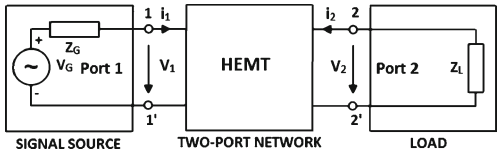

Figure 7. HEMT in two-port network.

(MAG/MSG), Rollett stability factor (K), Masons unilateral gain (MUG) and current gain (h_{21}) as a function of frequency are obtained as follows [17,18]:

The transconductance characterizes the current carrying capability of the device. Here the extrinsic transconductance of the proposed device is measured by varying the gate voltage (V_{gs}) from -1 V to 0.5 V when the drain–source voltage (V_{ds}) $= 1$ V. As seen in figure 8, the Si_3N_4-passivated device exhibits a maximum transconductance (g_m) of 131.7 mS/mm at the gate voltage of -0.354 V and SiO_2-passivated device exhibits a maximum transconductance of 114.6 mS/mm at the gate voltage of -0.4 V. It is realized that for better performance of the device, Si_3N_4 passivation layer is used because of its higher transconductance.

The maximum current gain cut-off frequency (f_t) and the maximum power gain cut-off frequency (f_{max}) are plotted in figures 9 and 10, as a function of bias for three different extraction methods such as unit-gain-point ($|h_{21}| = 1$), extract-at-dB Point (10 dB) and extract-at-frequency (10 GHz) of the two-port network set-up [17]. The maximum current gain cut-off frequencies (f_t) are 27.1 GHz and 23.97 GHz in unit-gain-point method at a gate voltage of -0.4 V for Si_3N_4 and SiO_2 passivation layers respectively. Similarly, the maximum power gain cut-off frequencies (f_{max}) are 41 GHz and 38.5 GHz in unit-gain-point method at a gate voltage of -0.1 V for Si_3N_4 and SiO_2 passivation layers

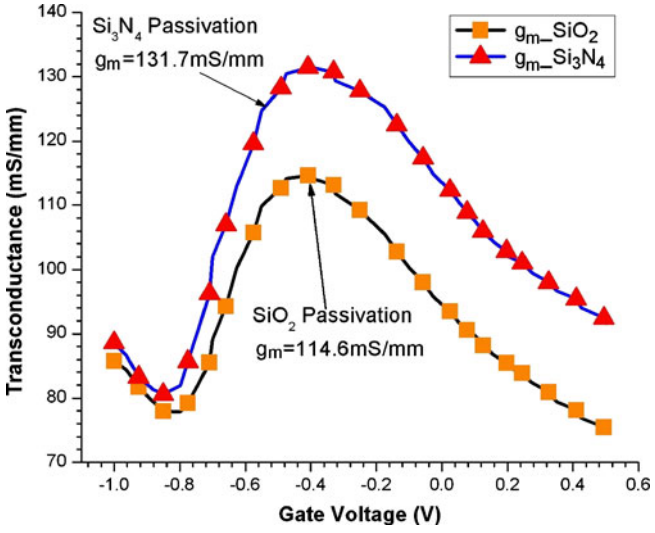

Figure 8. Extrinsic transconductance for Si_3N_4 and SiO_2 passivation layers.

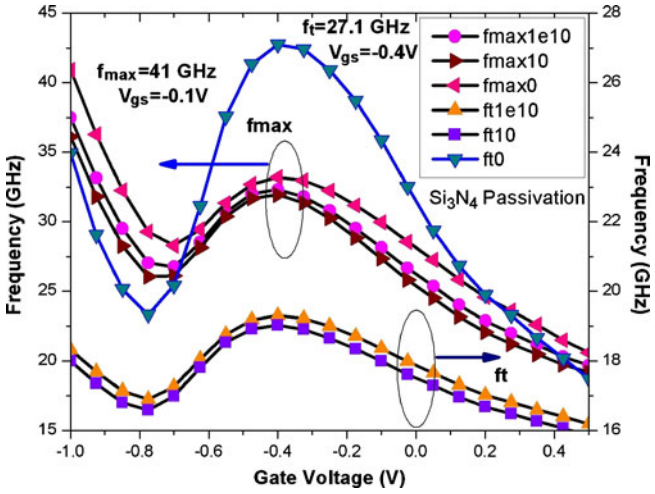

Figure 9. Maximum frequency of oscillation (f_{max}) and cut-off frequency (f_t) for Si_3N_4 passivation.

respectively. From these two results we can make out that better performance is achieved by using in Si_3N_4 passivation layer (shown in figure 10).

Figure 11 shows the frequency dependence of maximum available/stable gain (MAG/MSG) [18] for Si_3N_4 and SiO_2 passivation layers. From both the gain factors, it is realized that Si_3N_4 passivation layer gives better performance than the SiO_2 passivation layer with the variation of frequency from 100 MHz to 1 THz. According to the standard criterion of stability, i.e., when Rollett stability, $K > 1$, the HEMT is stable unconditionally and it indicates conjugate matching between output and input loads, and when

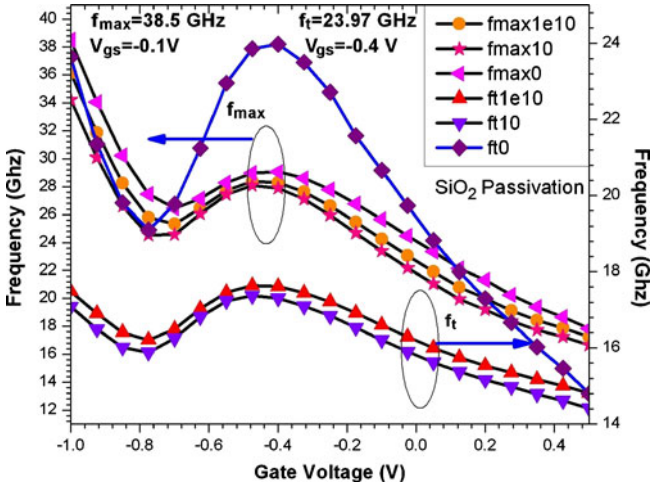

Figure 10. Maximum frequency of oscillation (f_{max}) and cut-off frequency (f_t) for SiO_2 passivation layer.

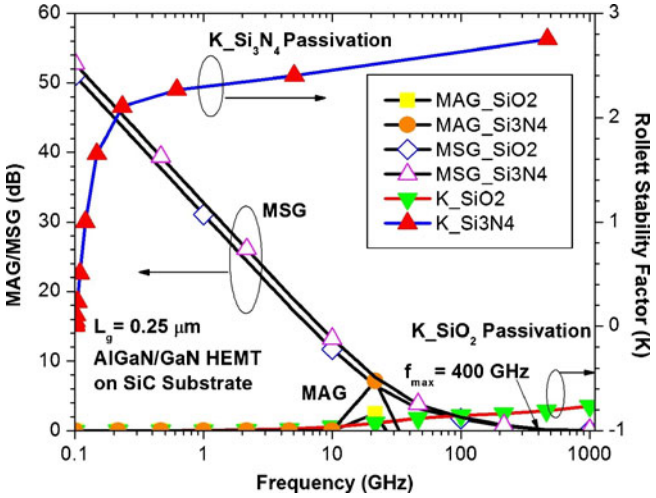

Figure 11. MAG/MSG for Si_3N_4 and SiO_2 passivation layers showing the stability.

$K < 1$, the circuit is conditionally stable [18]. From figure 11, it is clear that the HEMT, passivated with Si_3N_4 layer is stable unconditionally with the variation of frequency, i.e. in high frequency and when the HEMT is passivated with SiO_2 layer, it is conditionally stable in microwave frequency range because $K < 1$. The maximum stable gains for both passivated layer devices are maximum around 52 dB at 100 MHz and the unit gain (MSG = 1) is achieved at a frequency of 400 GHz as shown in figure 11.

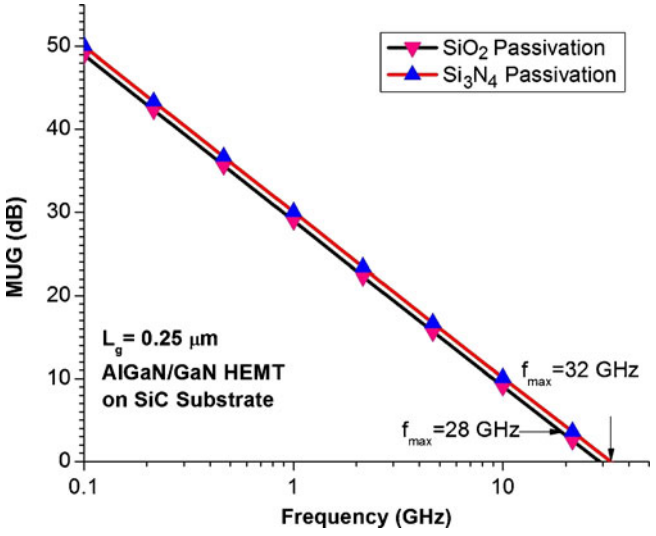

Figure 12. MUG for Si_3N_4 and SiO_2 passivation layers showing unit power gain cut-off frequency.

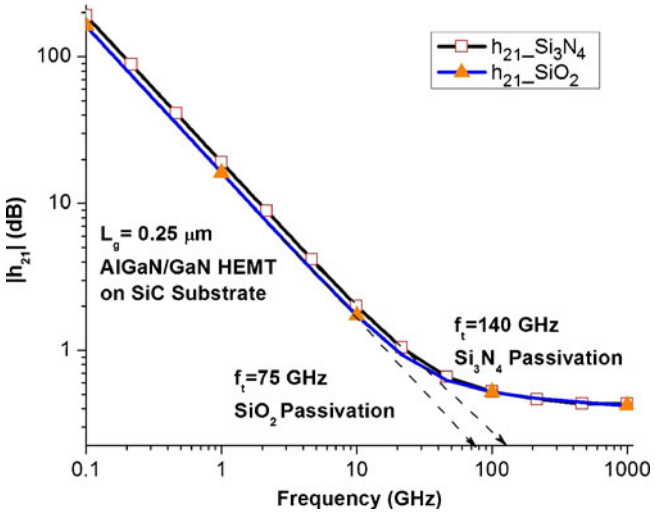

Figure 13. *Abs* $|h_{21}|$ for Si_3N_4 and SiO_2 passivation layers showing unit current gain cut-off frequency.

Similarly, the unit power gain (MUG = 1) cut-off frequency (f_{max}) is plotted in figure 12 from a family of Mason's unilateral gain (MUG) curves for both passivated devices. The maximum frequencies of oscillation are measured to be 32 GHz and 28 GHz for Si_3N_4 and SiO_2 passivation layer devices. Furthermore, the absolute $|h_{21}|$ current gains as a function of frequency up to 1 THz are plotted in figure 13 for Si_3N_4 and SiO_2 passivation layer devices. The unit-current gain cut-off frequencies are measured to be 140 GHz and 75 GHz by extrapolating 20 dB/decade for Si_3N_4 and SiO_2 passivation layer devices respectively. The comparative performance evaluation of gate-recessed AlGaN/GaN-based HEMT on SiC substrate using different passivation layers are given

Table 4. Comparative performance parameters of GaN-based HEMT using different passivation layers.

Factors	Si_3N_4 Passivation	SiO_2 Passivation
Drain current from gate characteristics ($I_{d,max}$)	290.2 mA/mm	263.5 mA/mm
Saturated drain current from drain characteristics ($I_{d,sat}$)	600 mA/mm	550 mA/mm
Transconductance parameter (g_m)	131.7 mS/mm	114.6 mS/mm
Cut-off frequency (f_t)	27.1 GHz	23.97 GHz
Maximum frequency of oscillation (f_{max})	41 GHz	38.5 GHz
Unit power gain cut-off frequency (f_{max}) from MUG curves	32 GHz	28 GHz
Unit current gain cut-off frequency (f_t) from $\|h_{21}\|$ curves	140 GHz	75 GHz
Stability	Unconditionally ($K > 1$)	Conditionally ($K < 1$)

in table 4 and it is noteworthy to mention that Si_3N_4 passivation layer device shows better performance in all aspects than SiO_2 passivation layer device.

5. Conclusion

The proposed AlGaN/GaN-based HEMT on SiC substrate is characterized by deploying Si_3N_4 and SiO_2 passivation layers. The gate length of the device is 0.25 μm. The device demonstrates an improved transconductance of 131.7 mS/mm for Si_3N_4 passivation layer and 114.6 mS/mm for SiO_2 passivation layer. The maximum current gain cut-off frequency $f_t = 27.1$ GHz and the maximum power gain cut-off frequency $f_{max} = 41$ GHz for Si_3N_4 passivation layer. The maximum frequencies of oscillation from MUG curves are also measured to be 32 GHz and 28 GHz for Si_3N_4 and SiO_2 passivation layer devices. Similarly, the unit current gain, $|h_{21}| = 1$ cut-off frequencies are measured to be 140 GHz and 75 GHz for Si_3N_4 and SiO_2 passivation layer devices respectively from the $abs\ |h_{21}|$ curves. When the device is passivated with Si_3N_4 layer, it is stable unconditionally with the variation of frequency towards 1 THz range. It is concluded that Si_3N_4 passivation layer gives better performance rather than its counterpart. The deposition of the Si_3N_4 passivation beside the gate has many advantages such as better sidewall coverage, less dispersion and easier field plate technology in deep-submicron devices.

Acknowledgements

The authors acknowledge the DST-SERC fund received by NIST from the Department of Science & Technology (DST), Govt. of India and also the School of Physics, Sambalpur University for providing the necessary facilities for carrying out this research work.

References

[1] S Khandelwal, N Goyal and Tor A Fjeldly, *IEEE Trans. Electron Devices* **58**, 3622 (2011)
[2] Zhang Renping and Yan Wei, *J. Semicond.* **32**, 1 (2011)
[3] Liu Guo-Guo and Wei Ke, *J. Infrared Millim. Waves* **30**, 289 (2011)
[4] Jinwook W Chung *et al*, *IEEE Electron Device Lett.* **31**, 195 (2010)
[5] Haifeng Sun *et al*, *Int. J. Microwave Wireless Technol.* **2**, 33 (2010)
[6] J Y Shiu *et al*, *Semicond. Sci. Technol.* **22**, 717 (2007)
[7] T R Lenka and A K Panda, *Semiconductors* **45**, 660 (2011)
[8] Jing Lu and Yan Wang, *Solid State Electron.* **52**, 115 (2008)
[9] Kim Bong-Hwan *et al*, *Chin. Phys. Lett.* **27**, 118501:1 (2010)
[10] Bruce M Green *et al*, *IEEE Electron Device Lett.* **21**, 268 (2000)
[11] A Brannick and N A Zakhleniuk, *Microelectron. J.* **40**, 410 (2009)
[12] W Luo *et al*, *Front. Elect. Electron. Eng. China* **3**, 120 (2008)
[13] X Cheng, M Li and Y Wang, *IEEE Trans. Electron Devices* **56**, 2881 (2009)
[14] T R Lenka and A K Panda, *Indian J. Pure Appl. Phys.* **49**, 416 (2011)
[15] Han-Yin Liu *et al*, *IEEE Trans. Electron Devices* **58**, 4430 (2011)
[16] H Xing *et al*, *J. Phys.: Condens. Matter* **13**, 7139 (2001)
[17] T R Lenka and A K Panda, *Semiconductors* **45**, 1211 (2011)
[18] R S Carson, *High-frequency amplifiers*, 2nd edn (John Wiley & Sons, Hoboken, NJ, 1982)